On Cooperative Broadcast in MANETs with Imperfect Clock Synchronization

Serdar Şahin*†, Antonio Maria Cipriano*, Charly Poulliat† and Marie-Laure Boucheret†
* Thales Communications & Security, Gennevilliers, 92230, France, Email: surname.name@thalesgroup.com
† University of Toulouse, IRIT-ENSEEIHT, Toulouse, 31000, France, Email: surname.name@enseeiht.fr

***Abstract*—This paper considers the evaluation of the characteristics of the channel that arises in the context of cooperative broadcast in mobile ad-hoc networks (MANETs) with practical radios, and tackles the problem of detection with affordable frequency domain receivers. When multiple nodes use cooperative signalling to transmit a signal to a destination, their clock offsets, oscillator drifts, and non-negligible propagation delays yield an equivalent doubly-selective channel seen from any destination node's point-of-view. For demanding applications with high data rate requirements, this equivalent cooperative channel needs to be mitigated with physical layer signal processing. In the first part of the paper, statistical characteristics of the power-delay profile of the equivalent cooperative transmission channel are modelled to gain a better understanding of its behaviour. This preliminary analysis points out that equalization is required to successfully carry out cooperative broadcast. Next, conventional linear frequency domain equalizer (FDE) and a recently proposed non-linear FDE based on Bayesian inference, are considered for the equalization of the aforementioned channels. The detection performance of these receivers is evaluated in some critical channels which can jeopardize the robustness of the cooperative links, identified with the preliminary statistical analysis. Numerical results indicate that, non-linear but low-complexity frequency domain receivers are attractive solutions for cooperative broadcast, especially within high-data rate applications.**

I. Introduction

The design of robust wireless mobile ad-hoc networks (MANETs) is of interest for many applications such as sensor, tactical or unmanned aerial vehicle (UAV) networks. Although the specific quality-of-service requirements for these applications differ, low latency and robust connectivity are common prerequisites for such decentralized infrastructures. Physical layer (PHY) design is particularly challenging for ground-to-ground tactical networks which involve hostile propagation environments with scattering and mobility.

The broadcast nature of wireless radio channels in MANETs is a gift, due to improved spectral-efficiency when distributing a packet from one node to neighbouring nodes, but it is also a curse due to the increased contention periods for avoiding excessive interference [1]. Traditional approaches [2] are built on naive flooding, which is robust but resource-inefficient, and several improvements use neighbourhood knowledge to identify and select relays to improve flooding efficiency.

In [3], accumulative broadcast was considered for minimum-energy broadcasting in loosely-synchronized networks with limited local information, thanks to the use of selective decode-and-forward [4]. Other approaches [5], [6] use simultaneous participation (i.e. non-orthogonal access) of multiple nodes for the re-transmission of a broadcast packet, which is referred to as *cooperative broadcast*. Such techniques are attractive for MANETs [7]. However non-orthogonal cooperative broadcast generates at the receiver an artificial multi-path channel given by the combinations of the signals from all active relays, thus potentially increasing the frequency selectivity perceived by the receiver.

Stochastic behaviour of multi-hop networks with cooperative broadcast is evaluated with the assumption of infinite nodes with finite power per area in [8]. Recent models for finite node densities [9]–[11] investigate on inter-node distance distributions and path-loss to evaluate range improvements brought by the cooperative broadcast. These works assume that transmitted signals coherently combine at destinations, ignoring selective channels caused by propagation delays, clock offsets and oscillator drifts.

In [12], impact of propagation delays and delay dithering are studied for harvesting cooperative diversity as frequency diversity with a time-domain decision feedback equalizer (DFE). [13] considers multi-hop cooperative broadcasting without frame resynchronization at each hop, and it analyzes the evolution of time synchronization errors across hops. But this work does not consider the impact of path-loss, nor the equalization of the artificial channel.

The design of PHY layer receivers for handling cooperative broadcast detection has been addressed in [14]–[16]. A major concern common to these works is the mitigation of carrier frequency offsets (CFO) caused by clock synchronization issues. Nevertheless, these works either use time-domain serial DFE for single-carrier signalling [14], [16], or frequency-domain detection followed by serial DFE for multi-carrier signalling [15]. In all cases, equalization complexity is at least quadratic in block length due to DFE filter computation, and large-delay spreads would further complicate the design.

In this paper, the detection of non-orthogonal cooperative transmissions in practical MANETs is addressed. The system model is given in section II. First, unlike previous works, we provide, in section III, a statistical model of the frequency-selective channels created by cooperative broadcast in MANETs to evaluate the behaviour of channel characteristics and selectivity, and to assess their implications on receiver design. Then, the question of low-complexity frequency-domain equalization (FDE) of such channels is tackled in section IV, using off-the-shelf channel coding, with single-carrier (SC) block transmissions. More specifically we propose

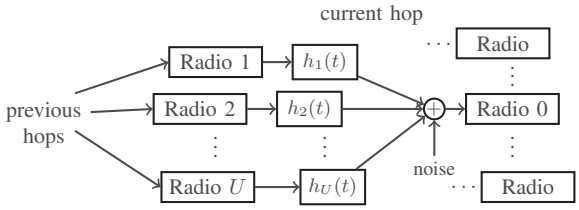

Fig. 1. Cooperative broadcast in a multi-hop MANET.

to compare conventional linear FDE (FD LE) performance with a recently proposed self-iterated linear FDE (FD SILE-EP) based on expectation propagation (EP), a technique for approximate Bayesian inference [17], [18]. Finally, in section V, we identify some critical configurations where the impact of the cooperative channel endangers the robustness of the physical link, for the case of a ground-to-ground tactical channel and an air-to-air UAV channel. The considered equalizers are evaluated from different perspectives in these channels.

II. Network and Channel Model

A MANET with homogeneous selective decode-and-forward [4] radios is considered within a cooperative broadcast framework. A source node transmits its codeword to all radios, and neighbouring nodes attempt to decode the message. Successful nodes (detected with a cyclic-redundancy code (CRC) check) simultaneously transmit the source codeword on the same time and frequency resource to the destinations of the current hop. The focus of this paper are PHY layer issues arising from such transmissions; U nodes of the current hop are relays, and a destination node (among others) indexed $u = 0$, attempts to decode it, as shown in Fig. 1.

A. Physical Channel Model

This section gets into details of the physical channel modelling for describing cooperative transmissions, by considering both large-scale and small-scale propagation effects. In the following, the position of the u^{th} radio is denoted p_u.

1) Large-Scale Effects: Large-scale propagation typically involves path-loss and shadowing, depending on the terrain and the nodes' positions. The focus of this study is on average channel behaviour, hence shadowing is averaged out. The path-loss component is $h_u^{\text{PL}} \triangleq 10^{-\text{PL}_u/10}$, with the log-domain path-loss in dB between the destination and the radio u being

$$\text{PL}_u = \text{PL}_{\text{ref}} + 20\log_{10}(f_c) + 10\alpha\log_{10}(d_u/d_{\text{ref}}), \quad (1)$$

where the distance d_u of the u^{th} node to the destination is $d_u \triangleq |p_0 - p_n|$, f_c is the carrier frequency and PL_{ref} and d_{ref} are large-scale channel parameters. The propagation delay between the transmitter u and the destination is denoted $\tau_u^{\text{prp}} \triangleq d_u/c$, where the speed of light is $c = 3 \times 10^8$ m/s. Hence the large-scale model between u^{th} node and the destination is

$$h_{\text{LS},u} = h_u^{\text{PL}}\delta(t - \tau_u^{\text{prp}}), \quad (2)$$

where $\delta(.)$ is the Dirac delta function.

2) Small-Scale Effects: Time and frequency selectivity caused by scattering and reflections are typically modelled by small-scale propagation components, and they are considered to be independent and identically distributed for all links. It is modelled as a time-varying L_{SS}-tap finite-impulse response

$$h_{\text{SS},u}(t) = \textstyle\sum_{l=0}^{L_{\text{SS}}-1} a_{\text{SS},l,u}(t)\delta(t - \tau_{\text{SS},l}), \quad (3)$$

where the Dirac delta function is denoted by δ, with power-delay profile $\{m_{\text{SS},l}, \sigma^2_{\text{SS},l}, \tau_{\text{SS},l}\}_{l=0}^{L_{\text{SS}}-1}$. Each tap l is a complex Gaussian process $a_{\text{SS},l,u}(t) \sim \mathcal{CN}(m_{\text{SS},l}, \sigma^2_{\text{SS},l})$, $\forall t$, $\forall u$, and $m_{\text{SS},l} = \sqrt{K_{\text{SS},l}\sigma^2_{\text{SS},l}}$, with $K_{\text{SS},l}$ being this tap's Rice factor, and $\mathcal{E}_{\text{SS},l} \triangleq m^2_{\text{SS},l} + \sigma^2_{\text{SS},l}$. Time-selective behaviour of each tap is specified by the Doppler spectrum $f \mapsto S_{\text{SS},l}(f)$. These parameters configure the nature of the small-scale channel.

3) Radio Characteristics: All transmitters use the same effective isotropic radiated power (EIRP), denoted $\mathcal{E}_{\text{tx}}$, which includes transmit antenna gain and amplifier back-off. We aim to characterize the artificial cooperative channel power delay profile (PDP), considering the transmit EIRP, average channel gains and delays. Following a network-wide synchronization procedure, each node has its internal clock shifted by a residual offset of t_u^{off} seconds with respect to an ideal global reference clock. Moreover, oscillator imperfections cause a frequency drift of f_u^{off} Hertz with respect to the carrier frequency f_c.

Considering these parameters, the channel between u^{th} node and the destination's antenna output is

$$h_u(t) = \sqrt{\mathcal{E}_{\text{rx},u}}e^{j2\pi t\phi_u}\textstyle\sum_{l=0}^{L_{\text{SS}}-1} a_{\text{SS},l,u}(t)\delta(t - \tau_{\text{SS},l} - \tau_u), \quad (4)$$

where the total delay between radios is $\tau_u \triangleq \tau_u^{\text{clk}} + \tau_u^{\text{prp}}$, with the component due to clock offsets being $\tau_u^{\text{clk}} \triangleq t_u^{\text{off}} - t_0^{\text{off}}$ and the carrier offset frequency being $\phi_u \triangleq f_u^{\text{off}} - f_0^{\text{off}}$. The received power from u^{th} user is $\mathcal{E}_{\text{rx},u} \triangleq \mathcal{E}_{\text{tx}}h_u^{\text{PL}}$.

Then, by combining the U cooperating transmitters, the cooperative broadcast channel is given by

$$h(t) = \textstyle\sum_{l=0}^{L-1} a_{l_l,l_u}(t)\delta(t - \tau_{l_l,l_u}), \quad (5)$$

where $l_u \triangleq \lceil (l+1)/L_{\text{SS}} \rceil$, $l_l \triangleq l \bmod L_{\text{SS}}$, $\tau_{l,u} \triangleq \tau_{\text{SS},l} + \tau_u$, $L = UL_{\text{SS}}$ and $a_{l,u}(t) \triangleq \sqrt{\mathcal{E}_{\text{rx},u}}e^{j2\pi t\phi_u}a_{\text{SS},l,u}(t)$. Impact of pulse-shaping filters, sampling and synchronization will be considered in section IV where PHY layer is discussed.

The cooperative transmission diversity presents itself in eq. (5) as supplementary frequency diversity, and, if paths are resolvable, it can to be harvested through equalization. However, equalization success depends on the frequency selectivity of the channel, which can be assessed with the delay spread

$$\Delta\tau = \Delta\tau_{\text{SS}} + \Delta\tau_{\text{prp}} + \Delta\tau_{\text{clk}}, \quad (6)$$

where the small-scale delay spread is $\Delta\tau_{\text{SS}} \triangleq \max_l \tau_{\text{SS},l} - \min_l \tau_{\text{SS},l}$ and the delay spread component caused by large-scale propagation is $\Delta\tau_{\text{prp}} = \max_u \tau_u^{\text{prp}} - \min_u \tau_u^{\text{prp}}$ and the one due to clock effects is $\Delta\tau_{\text{clk}} = \max_u \tau_u^{\text{clk}} - \min_u \tau_u^{\text{clk}}$.

The ability to equalize the channel also strongly depends on the dynamic power range of the channel, i.e. expected value of power differences between taps, which is defined in dB as

$$\Delta P \triangleq \Delta P_{\text{SS}} + \Delta P_{\text{prp}}, \quad (7)$$

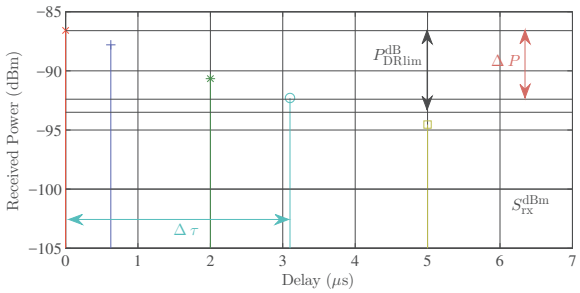

Fig. 2. A cooperative channel profile with 5 users (each colour is a user).

with $\Delta P_{\text{prp}} = \max_u 10\log_{10}(\mathcal{E}_{\text{rx},u}) - \min_u 10\log_{10}(\mathcal{E}_{\text{rx},u})$, and $\Delta P_{\text{SS}} = \max_l 10\log_{10}(\mathcal{E}_{\text{SS},l}) - \min_l 10\log_{10}(\mathcal{E}_{\text{SS},l})$.

As $\Delta\tau$ increases, and ΔP decreases, the inter-symbol interference caused by the channel become more severe. ΔP and $\Delta\tau$ above describe the frequency-selectivity of the cooperative channel with dependence on topology and radios, but some practical limitations at the receiver were omitted.

Indeed, strongly attenuated taps do not impact the frequency-selectivity, hence denoting the received power in dBm $\mathcal{E}^{\text{dBm}}_{\text{rx},u}$, only taps received from users such that

$$\mathcal{E}^{\text{dBm}}_{\text{rx},u} \geq S^{\text{dBm}}_{\text{rx}}, \tag{8}$$

will be relevant for computing ΔP and $\Delta\tau$. The receiver sensitivity in dBm is $S^{\text{dBm}}_{\text{rx}} \triangleq N_0 - 10\log_{10}(T_s) + L_{\text{r}}$, where N_0 is the noise power spectral density at receiver antenna in dBm/Hz, T_s is the symbol period, L_{r} is a constant in dB, including effects of antenna gains, noise figure and the detection threshold at the receiver.

Moreover, in the presence of strong taps, smaller channel components lose their impact and can even become neglected in receiver channel estimation algorithms. To account for such issues, a constraint on the dynamic range is added

$$\Delta P \leq P^{\text{dB}}_{\text{DRlim}}, \tag{9}$$

for evaluating the channel selectivity.

Fig. 2 illustrates these quantities on an instance of a cooperative broadcast channel with non-frequency-selective small-scale components. Alternatively, Fig. 2 can be understood as the representation of the influence of the delay spread component $\Delta\tau_{\text{prp}}$ caused by large-scale propagation. However this case is not restrictive, as the small-scale profile is independent, and its impact can be incorporated separately.

III. Statistical Behaviour of the Frequency-Selective Cooperative Channel

In this section, statistical characteristics of the cooperative channel in eq. (5), is assessed by assuming emitting node positions and radio imperfections are randomly distributed.

In the following, $p(X)$ denotes the probability density function (PDF) of the random variable X. Emitting nodes $1,\ldots,U$ are uniformly distributed on an annulus, centered on the destination node $u=0$, with an outer radius of d_0 meters and the width of the annulus is given by $r < d_0$, i.e. the inner

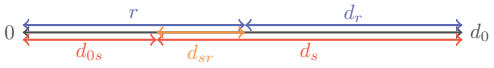

Fig. 3. Topology model illustration.

radius is $d_r \triangleq d_0 - r$. This is equivalent to a one-dimensional model where the destination is located at d_0 and emitters are uniformly distributed on the segment $[0, r]$, shown in Fig. 3. Moreover t^{off}_u is uniformly distributed on $[-\tau_{\text{clk}}/2, \tau_{\text{clk}}/2]$, with τ_{clk} setting the maximum absolute value of $\Delta\tau_{\text{clk}}$.

A. Frequency-Selective Characteristics

Here the PDFs of the $\Delta\tau$ and ΔP are exposed, without including small-scale effects. Detailed derivations are not given due to lack of space, but a sketch of proof is provided.

$\Delta\tau_{\text{prp}}$ and ΔP, tied to radio distance distributions, and the clock offset component $\Delta\tau_{\text{clk}}$ can be modelled separately, using change of variables on uniform and general Beta distributed random variables. However this approach does not consider the practical constraints in eqs. (8)-(9).

The dynamic range constraint (eq. (9)) is relevant on short distances, which is out of focus in this paper, hence only the impact of receiver sensitivity in eq. (8) is considered. The latter is equivalent to ignoring radios farther than d_s to radio 0, with

$$d_s = d_{\text{ref}} 10^{(\mathcal{E}_{\text{tx}} - S_{\text{rx}} - P_{\text{ref}} - 20\log_{10}(f_c))/(10\alpha)}. \tag{10}$$

Thus, $\Delta\tau_{\text{prp}}$ and ΔP_{prp} are defined with respect to constrained minimum and maximum distances $d_m \triangleq \min_{u,d_u<d_s} d_u$ and $d_M \triangleq \max_{u,d_u<d_s} d_u$. When $d_s < d_0$, $\Delta\tau_{\text{prp}}$ and ΔP_{prp} are non-zero iff at least two radios are in $[d_{0s}, r]$, $d_{0s} = d_0 - d_s$. The probability of having less than two users in this segment is $p_{0s} = d_{0s}^{U-1}(r + (U-1)d_{sr})/r^U$, with $d_{sr} = d_s - d_r$.

Finally, $\Delta\tau_{\text{prp}}$ and $\Delta\tau_{\text{clk}}$ are combined to model the PDF of the total delay spread $\Delta\tau$. To this end, the method used in [19] is generalized here with truncated general Beta random variables to obtain analytical expression of $p(\Delta\tau)$.

Following computations, the distribution of ΔP is given by

$$p(\Delta P) = \frac{\log 10}{10\alpha}\frac{(U-1)}{r^U}\frac{d_0^U - d_r^U 10^{\frac{U\Delta P}{10\alpha}}}{10^{\frac{\Delta P}{10\alpha}}\left(1 - 10^{\frac{-\Delta P}{10\alpha}}\right)^{2-U}}, \tag{11}$$

for $0 < \Delta P \leq 10\alpha\log_{10}(d_0/d_r)$, when $d_s \geq d_0$, and when $d_r < d_s < d_0$, ΔP follows

$$p(\Delta P) = p_{0s}\delta(0) + \frac{\log 10}{10\alpha}\frac{10^{\frac{\Delta P}{10\alpha}}}{\left(10^{\frac{\Delta P}{10\alpha}} - 1\right)^2}\frac{1}{r^U}\times \\ [(U-1)\varphi(\Delta P, U) - U d_{0s}\varphi(\Delta P, U-1)], \tag{12}$$

for $0 < \Delta P \leq 10\alpha\log_{10}(d_s/d_r)$, with

$$\varphi(x,u) = \left(d_0 - d_s 10^{\frac{-x}{10\alpha}}\right)^u - \left(r - d_s + d_r 10^{\frac{x}{10\alpha}}\right)^u.$$

The analytical expression of $\Delta\tau$'s PDF is given in eqs. (13)-(14), on the next page. The small-scale effects can be incorporated by translating these PDFs by ΔP_{SS} and by $\Delta\tau_{\text{SS}}$.

For $d_s > d_0$, the delay spread follows

$$p(\Delta\tau) = \begin{cases} \dfrac{\Delta\tau^{2U-3}(\tau_m-\Delta\tau)B(U-1,U-1)}{\tau_m^U\tau_M^{U-1}B(U-1,2)^2}F_1\left(\dfrac{\Delta\tau}{\Delta\tau-\tau_m},\dfrac{\Delta\tau}{\tau_M};U-1;-1,-1:2U-2\right) & \text{for } 0\le\Delta\tau\le\tau_m \\ \dfrac{(\Delta\tau-\tau_m)^{U-2}(\tau_t-\Delta\tau)}{\tau_M^U B(U-1,2)}F_1\left(\dfrac{\tau_m}{\tau_m-\Delta\tau},\dfrac{\tau_m}{\tau_t-\Delta\tau};2;2-U,-1;U+1\right) & \text{for } \tau_m<\Delta\tau\le\tau_M \\ \dfrac{(\tau_t-\Delta\tau)^3(\Delta\tau-\tau_m)^{U-2}}{6\tau_m^2\tau_M^U B(U-1,2)^2}F_1\left(\dfrac{\tau_t-\Delta\tau}{\tau_m},\dfrac{\Delta\tau-\tau_t}{\Delta\tau-\tau_m};2;2-U,2-U;4\right) & \text{for } \tau_M<\Delta\tau\le\tau_t \end{cases} \quad (13)$$

with $\tau_m = \min(\tau_r, \tau_{\text{clk}})$, $\tau_M = \max(\tau_r, \tau_{\text{clk}})$, $\tau_r = r/c$, $\tau_t = \tau_m + \tau_M$, and $F_1(x, y; a; b_1, b_2; c)$ is the Appell hypergeometric series of the first kind, and $B(\alpha, \beta)$ is the beta function, and for $d_r < d_s < d_0$, $p(\Delta\tau) = p_{0s}\delta(0) + p'(\Delta\tau)$ with

$$p'(\Delta\tau) = \begin{cases} \dfrac{\tau_{0s}^{U-2}\tau_{sr}\Delta\tau^{U-1}}{\tau_r^U\tau_{\text{clk}}^U B(U-1,2)}\left[\begin{array}{l}\Delta\tau F_1\left(\dfrac{-\Delta\tau}{\tau_{0s}},\dfrac{\Delta\tau}{\tau_{sr}};2;2-U,-1:U+1\right)+\\ U(\tau_{\text{clk}}-\Delta\tau)F_1\left(\dfrac{-\Delta\tau}{\tau_{0s}},\dfrac{\Delta\tau}{\tau_{sr}};1;2-U,-1:U\right)\end{array}\right] & \text{for } 0\le\Delta\tau\le\min(\tau_{\text{clk}},\tau_{sr}) \\ \dfrac{(\Delta\tau-\tau_{ms})^{U-2}(\tau_{ts}-\Delta\tau)}{\tau_r^U B(U-1,2)}F_1\left(\dfrac{\tau_{\text{clk}}}{\tau_{ms}-\Delta\tau},\dfrac{\tau_{\text{clk}}}{\tau_{ts}-\Delta\tau};2;2-U,-1;U+1\right) & \text{for } \tau_{\text{clk}}<\Delta\tau\le\tau_{sr} \\ \dfrac{\tau_{sr}^2(\Delta\tau-\tau_{ts})^{U-2}}{6\tau_r^2\tau_{\text{clk}}^U B(U-1,2)^2}\left[\begin{array}{l}\tau_{sr}F_1\left(\dfrac{\tau_{sr}}{\tau_{sr}-\Delta\tau},\dfrac{\tau_{sr}}{\tau_r};2;2-U,2-U:4\right)+\\ 3(\tau_{\text{clk}}-\Delta\tau)F_1\left(\dfrac{\tau_{sr}}{\tau_{sr}-\Delta\tau},\dfrac{\tau_{sr}}{\tau_r};2;2-U,2-U:3\right)\end{array}\right] & \text{for } \tau_{sr}<\Delta\tau\le\tau_{\text{clk}} \\ \dfrac{(\tau_{ts}-\Delta\tau)^3(\Delta\tau-t_{ms})^{U-2}}{6\tau_{\text{clk}}^2\tau_r^U B(U-1,2)^2}F_1\left(\dfrac{\tau_{ts}-\Delta\tau}{\tau_{\text{clk}}},\dfrac{\Delta\tau-\tau_{ts}}{\Delta\tau-\tau_{ms}};2;2-U,2-U;4\right) & \text{for } \max(\tau_{\text{clk}},\tau_{sr})<\Delta\tau\le\tau_{ts} \end{cases} \quad (14)$$

with $\tau_{ts} = \tau_{\text{clk}} + \tau_{sr}$, $\tau_{ms} = \tau_{\text{clk}} - \tau_{0s}$, $\tau_{sr} = d_{sr}/c$, $\tau_{0s} = d_{0s}/c$. For $d_s < d_r$, the delay spread is zero, i.e. $p(\Delta\tau) = \delta(0)$.

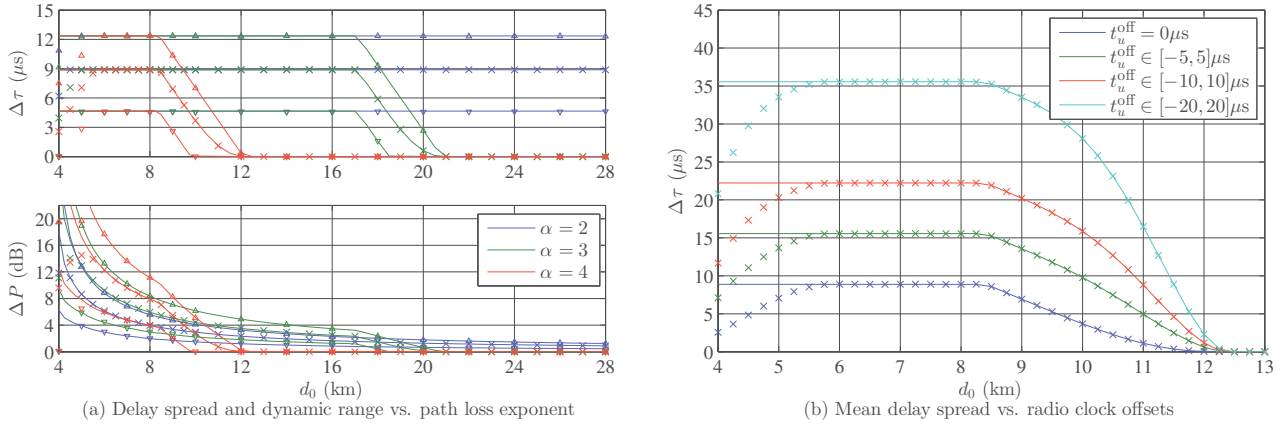

(a) Delay spread and dynamic range vs. path loss exponent

(b) Mean delay spread vs. radio clock offsets

Fig. 4. Mean value and quantiles of the delay spread and the dynamic range versus destination distance d_0 (lines: predicted, markers: experimental).

B. Numerical results on frequency-selectivity

In this section the statistical model above is used to evaluate the behaviour of a subset of a MANET with $U = 5$ nodes and $r = 4$ km. We use typical wireless radio parameters $\mathcal{E}_{\text{tx}}^{\text{dBm}} = 45.5$ dBm, $S_{\text{rx}}^{\text{dBm}} = -100$ dBm, within the UHF band with $f_c = 400$ MHz, using a symbol period of $T_s = 1$ µs. Path-loss parameters are in part based on ITU-R P.1546-1 recommendations with $P_{\text{ref}} = -60$ dB, $d_{\text{ref}} = 1$ km.

Using the PDFs derived previously, the mean value, the 5% and 95% quantiles of the delay spread and the dynamic range are evaluated for varying d_0 and path-loss exponent α, without any clock imperfection. The results are plotted in Fig. 4-a with solid, dashed and dotted lines, respectively for the mean, the 95% and 5% quantiles. Analytical predictions are illustrated by Monte-Carlo simulation results with respectively cross, upward and downward triangle markers. Furthermore, for $\alpha = 4$, the impact of the clock offsets $t_u^{\text{off}} \in [-\tau_{\text{clk}}/2, \tau_{\text{clk}}/2]$ on the mean value of the delay spread is shown in Fig. 4-b.

Algorithm 1 Frequency Domain Self-Iterated Linear Equalizer based on Expectation Propagation (FD SILE-EP)

Input $\mathbf{y}_p$, $\hat{\mathbf{H}}_p$, σ_w^2

1: Apply N-point Fast Fourier transform (FFT) on $\mathbf{y}_p$ and $\hat{\mathbf{H}}_p$ to get $\underline{\mathbf{y}}_p$, $\underline{\hat{\mathbf{H}}}_p = \mathbf{diag}(\text{`}\underline{\hat{\mathbf{h}}}_p)$.
2: Initialize the mean and the variance of the demapper feedback $(\bar{\underline{\mathbf{x}}}_p^{(s=0)}, \bar{v}_p^{(s=0)})$ with $(\mathbf{0}_{N,1}, \sigma_x^2)$.
3: **for** $s = 0$ to $\mathcal{S}$ **do**
4: Compute FDE normalization factor $\bar{\xi}_p^{(s)} = N^{-1} \sum_{n=0}^{N-1} |\hat{\underline{h}}_{n,p}|^2 / (\sigma_w^2 + \bar{v}_p^{(s)} |\hat{\underline{h}}_{n,p}|^2)$.
5: Compute FDE output variance $\bar{v}_{e,p}^{(s)} = 1/\bar{\xi}_p^{(s)} - \bar{v}^{(s)}$, and equalizer taps $\underline{f}_{n,p}^{(s)} = \hat{\underline{h}}_{n,p} / [\bar{\xi}_p^{(s)} (\sigma_w^2 + \bar{v}^{(s)} |\hat{\underline{h}}_{n,p}|^2)], \forall n$.
6: Interference cancellation and filtering: $\hat{\underline{x}}_{n,p}^{(s)} = \bar{\underline{x}}_{n,p}^{(s)} + \underline{f}_{n,p}^{(s)*} (\underline{y}_{n,p} - \hat{\underline{h}}_{n,p} \bar{\underline{x}}_{n,p}^{(s)}), \forall n$, use N-point inverse FFT to get $\hat{\mathbf{x}}_p^{(s)}$.
7: Compute the distribution $\{\mathcal{D}_{n,p}(\alpha) \propto \exp(|\hat{x}_{n,p}^{(s)} - \alpha|^2) / \bar{v}_{e,p}^{(s)}\}_{\alpha \in \mathcal{X}}, \forall n$ and compute their mean $\mu_{n,p}^{(s)}$ and variance $\gamma_{n,p}^{(s)}$.
8: Compute average posterior variance $\bar{\gamma}_p^{(s)} = N^{-1} \sum_n \gamma_{n,p}^{(s)}$, and carry out Gaussian division to compute next iteration's demapper feedback variance $\bar{v}_p^{(s+1)} = \bar{v}_{e,p}^{(s)} \bar{\gamma}_p^{(s)} / (\bar{v}_{e,p}^{(s)} - \bar{\gamma}_p^{(s)})$, and means $\bar{x}_{p,n}^{(s+1)} = \bar{v}_p^{(s+1)} (\mu_{n,p} / \bar{\gamma}_p^{(s)} - \hat{x}_{n,p}^{(s)} / \bar{v}_{e,p}^{(s)}), \forall n$.
9: **end for**
10: Provide extrinsic outputs $L_e(\mathbf{d}_{n,p}), \forall n$ to the decoder, by bit-wise marginalization of the posterior distribution.

Proposed prediction model is accurate for medium to high distances, but experimental and predicted data diverge for small d_0, due to neglected constraint in eq. (9). Indeed, at low distances, the clipping effect of this constraint is seen on ΔP, as the 95% quantiles saturate near $P_{\text{DRlim}}^{\text{dB}} = 20$ dB. In medium distances, the delay spread reaches its topological maximum when it is neither constrained by eq. (8) nor eq. (9), and reaches the mean of the delay spread distribution, given by $\Delta\tau = (\tau_{\text{clk}} + \tau_r)(U-1)/(U+1)$, which yields $\Delta\tau = 8.89$ µs for $\tau_{\text{clk}} = 0$ µs. Finally at high distances, the delay spread decreases due to the constraint (8), which allows to neglect paths with received power below receiver sensitivity, i.e. without a significant impact on detection performance.

Although most cooperative broadcast analysis carried out in the literature are based on flat-fading assumptions, results above indicate that frequency selectivity caused by such transmissions can be severe, as $\Delta\tau$ increases and ΔP decreases. In particular, conclusions drawn on range-extension capabilities are likely far from reality, for medium to high data rate applications, as severe inter-symbol interference (ISI) is present.

In the following, we discuss low-complexity detection of cooperative broadcast transmissions in MANETs, with frequency domain equalization and off-the-shelf error correction codes.

IV. Detection for Cooperative Broadcasting

Considering the numerical results above indicating large delay spreads in Fig. 4, traditional time-domain strategies can have excessive computational costs [12], [14]. Usually in the context of large delays spreads, frequency domain equalization is preferable, and thus we propose to investigate a single-carrier FDE strategy in MANETs for cooperative broadcasting.

Nevertheless, considering potential oscillator drifts of cooperating nodes, caused by clock synchronization issues, an encoding strategy across multiple short data blocks is needed, for improved robustness against time variations of the channel.

In particular, a recently proposed iterative FDE based on EP, FD SILE-EP [18] will be compared to the conventional FD LE [20], to cope with high frequency-selectivity of the artificial channel generated by the cooperative broadcast.

A. PHY Structure with BICM

Single-carrier transmission of P blocks of N symbols is considered using a bit-interleaved coded modulation (BICM) scheme. In detail, an information block $\mathbf{b} \in \mathbb{F}_2^{K_b}$ is first encoded and then interleaved into P code blocks $\mathbf{d}_p \in \mathbb{F}_2^{K_d}$, $p = 0, \ldots, P-1$, where $\mathbb{F}_2$ denotes the binary Galois field, with code rate $R_c \triangleq K_b/(K_d P)$. A memoryless modulator φ maps each code block $\mathbf{d}_p$ into the data block $\mathbf{x}_p \in \mathcal{X}^N$, where $\mathcal{X}$ is the M^{th} order complex constellation with zero mean, and with average power $\sigma_x^2 = 1$, and where $N = K_d/q$, with $q \triangleq \log_2 M$. This operation maps the q-word $\mathbf{d}_{n,p} \triangleq [d_{qn,p}, \ldots, d_{q(n+1)-1,p}]$ to the symbol $x_{n,p}$.

Radios use pulse-shaped SC waveforms for transmitting coded blocks, with $h_{\text{ps}}(t)$ being the overall Nyquist filter response across the channel. The receiver re-samples observations at the baseband, with a synchronization algorithm which yields the sampling instant t_0 which maximizes the equivalent baseband channel energy. Thus down-sampled taps of the cooperative channel is given by $h_{k,l} \triangleq h(t_0 + (k+l)T_s)$, where T_s is the symbol period.

Physical channel evolves continuously across transmitted sub-blocks, i.e. they are not independent, but the receiver operates with the assumption of a static block fading channel, the impulse response $\hat{\mathbf{h}}_p = \left[\hat{h}_{0,p}, \ldots, \hat{h}_{L-1,p}\right]$, by using an ideal channel estimate sampled in the centre of sub-blocks.

Transmitted sub-blocks are preceded by appropriately dimensioned cyclic-prefixes; receiver perceives a baseband circular channel for the transmission of data block $\mathbf{x}_p$ with

$$\mathbf{y}_p \approx \hat{\mathbf{H}}_p \mathbf{x}_p + \mathbf{w}_p, \tag{15}$$

where $\hat{\mathbf{H}}_p \in \mathbb{C}^{N \times N}$ is a circulant matrix, generated by the impulse response $\hat{\mathbf{h}}_p$ extended with $N-L$ zeros, $L < N$ being the baseband channel spread. The noise at the receiver $\mathbf{w}_p$ is modelled as an additive white Gaussian noise $\mathcal{CN}(\mathbf{0}_N, \sigma_w^2 \mathbf{I}_N)$.

The baseband receiver consists of a detector-bank; each one of the P transmitted blocks is equalized, then demodulated to yield extrinsic bit log-likelihood ratios $L_e(\cdot)$ to the decoder.

The previously mentioned iterative FDE [21], consists of an equalization process which is followed by the computation

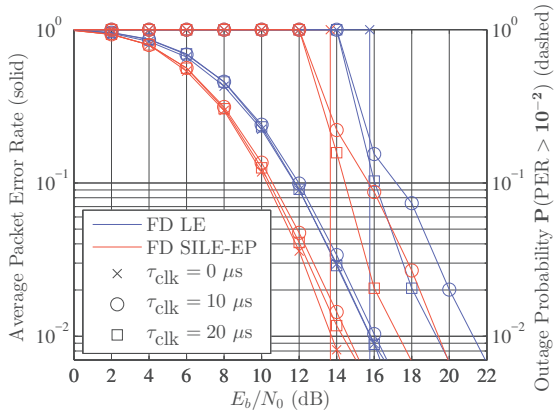

Fig. 5. Impact of clock offset in the tactical scenario with $R_c = 2/3$.

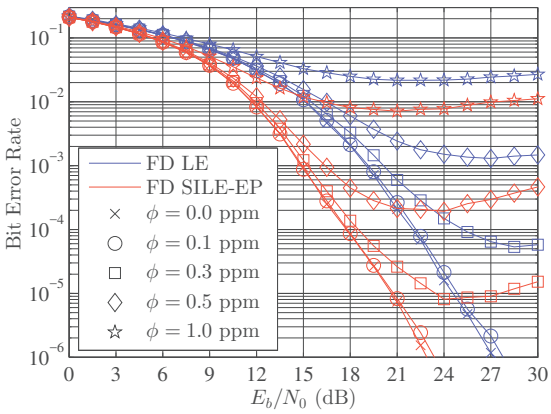

Fig. 6. Impact of CFO on the uncoded BER in the UAV scenario.

of an *extrinsic* soft feedback from the *demodulator*, which is fed back for interference cancellation and another round of equalization. Without self-iterations, this structure coincides with the conventional FD LE. More details on FD SILE-EP is available in [21], and an overview is given in Algorithm 1.

V. Numerical Results and Discussion

This section discusses numerical results on cooperative broadcast with the SC-FDE PHY detection strategy described above. In the following, we consider the transmission by $U = 5$ relays, with $r = 4$ km, of $P = 3$ blocks of $N = 128$ with 8-PSK modulation, using root-raised-cosine shaping filters with a roll-off of 0.35, $T_s = 1\mu$s, and using LTE channel coding and rate matching. The FD SILE-EP equalizer uses a linear feedback damping factor of 0.33 [18]. We focus on some test-bench channels which can affect the PHY layer link robustness, by using the results observed in Fig. 4.

A. Ground-to-ground tactical communications scenario

First, a ground-to-ground tactical MANET is considered with small-scale channel being a single-tap Rayleigh variable, and the path-loss exponent being $\alpha = 4$. For a destination located at $d_0 = 8$ km, the considered channel power profile $[0, -3.4, -6.2, -8.6, -10.8]$ in dB corresponds to the average topology yielding the 95%-quantile of delay spread ($\Delta\tau_{\mathrm{prop}} = 12\mu$s), i.e. equally 900m-spaced nodes. This exponentially decreasing channel is fairly easy to equalize, but radio clock offsets t_u^{off} increase the channel selectivity as observed in Fig 4-b, and they can cause a loss of frequency diversity, if delayed signals become un-resolvable.

In Fig. 5, the average packet error rate (PER) performance of FD LE and FD SILE-EP, with $R_c = 2/3$, is displayed in solid lines, by averaging over 150 realizations of uniformly distributed clock offsets, between $[-\tau_{\mathrm{clk}}/2, \tau_{\mathrm{clk}}/2]$, as in Fig 4-b. Some delay realizations which cause independent taps to become unresolvable cause significant diversity loss, but this only slightly degrades the *average* PER. Nevertheless, for considering the impact of clock offset realizations on the robustness of the average PER, the outage probability $\mathbb{P}[\mathrm{PER} > 10^{-2}]$ is evaluated and it is displayed in dashed lines. For $\tau_{\mathrm{clk}} = 0\mu$s, the outage only occurs when the average PER is lower than 10^{-2}, which yields a SNR threshold-like behaviour. It is seen that $\tau_{\mathrm{clk}} = 10\mu$s cause a significant loss of diversity, but this loss is smaller for $\tau_{\mathrm{clk}} = 20\mu$s. This behaviour is natural, as realizations with unresolvable taps become more unlikely as τ_{clk} increases too much.

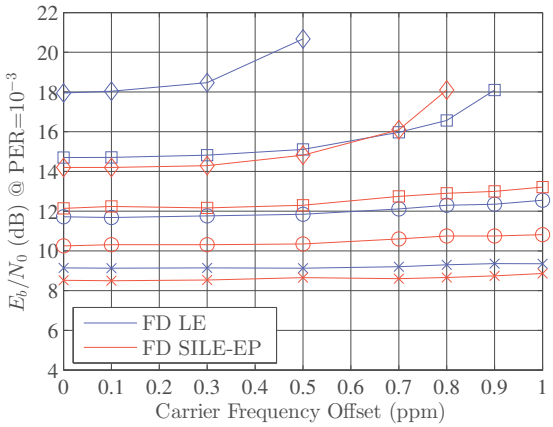

Fig. 7. Impact of CFO on the coded performance of the UAV scenario. $R_c = 1/3, 1/2, 2/3, 5/6$ are respectively denoted by $\times$, $\circ$, $\square$, $\diamond$.

B. Air-to-air UAV communications scenario

We now consider an intra-UAV communication scenario where the small-scale channel is single-tap with a Rice factor of 10 dB [22] and the path-loss exponent is $\alpha = 2$. As UAVs need to be equipped with precise localization systems (e.g. Global Positioning System - GPS), clock offset issues can be greatly reduced and enable good network-wide synchronization. Thus CFOs can realistically be controlled to remain less than a ppm. However, challenging receiving conditions may arise when non-negligible relays signals have significantly different CFOs, thus increasing the time-selectivity of the received signal. Considering a scenario with $d_{1:5} = [4.0, 2.5, 2.2, 0.7, 0.4]$ km, corresponding to a realization of

the 95%-quantile of $\Delta\tau_{\text{prop}}$, and $d_0 = 20$ km which yields the near-uniform power profile $[0, -0.78, -0.93, -1.6, -1.8]$ in dB, which is rich in diversity but difficult to equalize. For testing, we assume a worst case situation in which close nodes have very different CFOs, i.e. $\phi_{1:5} = [\phi, -\phi, \phi, -\phi, \phi]$.

In Fig. 6, uncoded bit error rate (BER) performance of considered equalizers is plotted. Increase in CFO is shown to create an error floor, which is then enhanced as the signal-to-noise ratio (SNR) increases, due to the channel estimate mismatch at the equalizer. In practice, the error-floor can be kept at its minimum, by accounting for the channel mismatch errors within the equalizer filters. It is seen that without CFO ($\phi = 0$ ppm), the FD SILE-EP brings around 4.2 dB gain over FD LE at BER=10^{-3}, and regardless of the CFO, FD SILE-EP has lower error floors and notable SNR gains. The $\phi = 1$ ppm case might be unrealistic for UAVs, but it allows assessing the limits of considered receiver.

Considering the same scenario with LTE channel coding for $R_c = [1/3, 1/2, 2/3, 5/6]$, the trade-off between higher throughput or a more powerful code is assessed in Fig. 7. The E_b/N_0 required to decode with PER=10^{-3} is plotted as a function of the CFO ϕ, for these code rates and the considered equalizers. For $\phi > 0.8$ ppm, both FDE cannot decode $R_c = 5/6$, and FD LE can no longer decode $R_c = 2/3$ for $\phi > 0.9$ ppm. Strong codes manage to cope with typical values of CFO, and FD SILE-EP bring small improvements, but with higher code rates the performance is severely degraded, and the benefits of using an iterative receiver, such as FD SILE-EP, is more significant. In particular, FD SILE-EP considerably improves spectral efficiency, as it decodes at $R_c = 5/6$ with better energy efficiency than FD LE operating at $R_c = 2/3$, up to $\phi = 0.7$ ppm.

VI. Conclusion

An analytical model is provided on the distribution of the delay spread and the dynamic range of cooperative broadcast channels that appear in MANETs with imperfect radio clock synchronization. This provides a means to assess the frequency selectivity of the artificial channels generated by such transmissions, and to design the PHY layer accordingly.

We have evaluated the performance of frequency-domain equalization for handling such transmissions in some scenarios of interest. Numerical results showed how radio imperfections could impact the link quality and that modern iterative frequency domain receivers could become viable solutions with significant advantages over conventional FDE, especially when dealing with high data rate transmissions. Our results assume the use of appropriately-sized cyclic prefixes, and this could lead to some loss of efficiency in certain scenarios. In such cases, the use of an iterative overlap FDE could be preferred, as shown in [21] for the case of mobile to mobile communications in a mountainous area.

Previous works on the analysis of cooperative broadcasting in MANETs often ignore the impact of the underlying artificial frequency-selective channel. This can potentially overestimate the performance prediction for practical applications if realistic low-cost radios are to be used. This paper aims to regain awareness in these issues, and future works will focus on assessing the impact of these PHY-layer considerations on higher layer quality-of-service metrics of MANETs.

References

[1] Y.-C. Tseng, S.-Y. Ni, Y.-S. Chen, and J.-P. Sheu, "The broadcast storm problem in a mobile ad hoc network," *Wireless Networks*, vol. 8, no. 2, pp. 153–167, Mar. 2002.

[2] B. Williams and T. Camp, "Comparison of broadcasting techniques for mobile ad hoc networks," in *Proceedings of the ACM MobiHoc'02*, New York, NY, USA, 2002, pp. 194–205.

[3] I. Maric *et al.*, "Cooperative multihop broadcast for wireless networks," *IEEE J. Sel. Areas Commun.*, vol. 22, no. 6, pp. 1080–1088, Aug. 2004.

[4] J. N. Laneman, D. N. C. Tse, and G. W. Wornell, "Cooperative diversity in wireless networks: Efficient protocols and outage behavior," *IEEE Trans. Inf. Theory*, vol. 50, no. 12, pp. 3062–3080, Dec. 2004.

[5] A. Scaglione *et al.*, "Opportunistic large arrays: cooperative transmission in wireless multihop ad hoc networks to reach far distances," *IEEE Trans. Signal Process.*, vol. 51, no. 8, pp. 2082–2092, Aug. 2003.

[6] G. Jakllari, S. V. Krishnamurthy, M. Faloutsos *et al.*, "A framework for distributed spatio-temporal communications in mobile ad hoc networks," in *Proc. IEEE INFOCOM'06*, Apr. 2006, pp. 1–13.

[7] R. Ramanathan, "Challenges: A radically new architecture for next generation mobile ad hoc networks," in *Proceedings of the ACM MOBICOM'05*, 2005, pp. 132–139.

[8] B. Sirkeci-Mergen, A. Scaglione, and G. Mergen, "Asymptotic analysis of multistage cooperative broadcast in wireless networks," *IEEE Trans. Inf. Theory*, vol. 52, no. 6, pp. 2531–2550, Jun. 2006.

[9] Ç. Çapar, D. Goeckel, and D. Towsley, "Broadcast analysis for extended cooperative wireless networks," *IEEE Trans. Inf. Theory*, vol. 59, no. 9, pp. 5805–5810, Sep. 2013.

[10] S. A. Hassan and M. A. Ingram, "On the modeling of randomized distributed cooperation for linear multi-hop networks," in *Proceedings of the IEEE ICC'12*, Jun. 2012, pp. 366–370.

[11] T. Rüegg, F. Gentile, and A. Wittneben, "Cooperative broadcast performance prediction based on inter-node distance distributions," in *Proc. of the IEEE WCNC'18*, Apr. 2018.

[12] S. Wei, D. L. Goeckel *et al.*, "Asynchronous cooperative diversity," *IEEE Trans. Wireless Commun.*, vol. 5, no. 6, pp. 1547–1557, Jun. 2006.

[13] M. Hussain and S. A. Hassan, "Performance of multi-hop cooperative networks subject to timing synchronization errors," *IEEE Trans. Commun.*, vol. 63, no. 3, pp. 655–666, Mar. 2015.

[14] D. Veronesi and D. L. Goeckel, "Multiple frequency offset compensation in cooperative wireless systems," in *Proceedings of the IEEE GLOBECOM'06*, Nov. 2006, pp. 1–5.

[15] N. Benvenuto, S. Tomasin, and D. Veronesi, "Multiple frequency offsets estimation and compensation for cooperative networks," in *Proceedings of the IEEE WCNC'07*, Mar. 2007, pp. 891–895.

[16] H. Wang *et al.*, "Computationally efficient equalization for asynchronous cooperative communications with multiple frequency offsets," *IEEE Trans. Wireless Commun.*, vol. 8, no. 2, pp. 648–655, Feb. 2009.

[17] T. P. Minka, "A family of algorithms for approximate Bayesian inference," Ph.D. dissertation, M.I.T., Jan. 2001.

[18] S. Şahin, A. M. Cipriano, C. Poulliat, and M.-L. Boucheret, "Iterative equalization based on expectation propagation: a frequency domain approach," in *Proc. IEEE 26th Eur. Signal Process. Conf.*, Sep. 2018.

[19] T. Pham-Gia and N. Turkkan, "Distribution of the linear combination of two general beta variables and applications," *Communications in Statistics - Theory and Methods*, vol. 27:7, pp. 1851–1869, 1998.

[20] H. Sari, G. Karam, and I. Jeanclaud, "Frequency-domain equalization of mobile radio and terrestrial broadcast channels," in *Proc. IEEE GLOBECOM'04*, Nov. 1994, pp. 1–5 vol.1.

[21] S. Şahin, A. Cipriano, C. Poulliat *et al.*, "A framework for iterative frequency domain EP-based receiver design," *IEEE Trans. Commun.*, Apr. 2018, to be published. [Online]. Available: https://ieeexplore.ieee.org/document/8426040/

[22] N. Goddemeier and C. Wietfeld, "Investigation of air-to-air channel characteristics and a UAV specific extension to the Rice model," in *IEEE Globecom Workshops*, Dec. 2015, pp. 1–5.